Diurnal and Semidiurnal Variations of the Surface Wind Field over the Tropical Pacific Ocean

CLARA DESER* AND CATHERINE A. SMITH

CIRES, University of Colorado, Boulder, Colorado

(Manuscript received 25 March 1997, in final form 17 August 1997)

ABSTRACT

The climatological large-scale patterns of diurnal and semidiurnal near-surface wind variations over the tropical Pacific Ocean are documented using 3 yr of hourly measurements from the Tropical Atmosphere–Ocean moored buoy array. Semidiurnal variations account for 68% of the mean daily variance of the zonal wind component, while diurnal variations account for 82% of the mean daily variance of the meridional wind component. The spatially uniform amplitude (0.15 m s^{-1}) and phase (0300 LT) of the semidiurnal zonal wind variations are shown to be consistent with atmospheric thermal tidal theory.

The diurnal meridional wind variations on either side of the equator are approximately out of phase. This pattern results in a diurnal variation of wind divergence along the equator, with maximum divergence in the early morning (~0800 LT). The average amplitude of the diurnal cycle in zonal mean divergence is 0.45×10^{-6} s^{-1}, which corresponds to a day–night change of 45% relative to the daily mean. The relative day–night changes in near-surface equatorial wind divergence are larger in the western Pacific (78%) than in the eastern Pacific (31%) due mainly to differences in the daily mean divergence. The diurnal amplitude of equatorial wind divergence changes seasonally and interannually in proportion to the strength of the mean divergence.

It is suggested that diurnal heating of the sea surface may contribute to the zonally symmetric diurnal cycle of equatorial wind divergence.

1. Introduction

Tropical meteorologists have long noted the existence of daily[1] variations in a variety of weather elements, including cloudiness, rainfall, and barometric pressure over the open ocean. Semidiurnal fluctuations have been identified most prominently in sea level pressure records (Haurwitz 1956; Haurwitz and Cowley 1973; Hamilton 1980), but also in tropospheric zonal winds (Nitta and Esbensen 1974; Pedder 1978; Morrissey 1990; Williams et al. 1992), light rain, and associated stratiform cloudiness (Rickenbach and Rutledge 1997, manuscript submitted to *J. Atmos. Sci.*, hereafter RR97). The classical theory of the atmospheric thermal tide accounts well for the zonally uniform phase and amplitude of the semidiurnal pressure changes within the Tropics (Lindzen 1968; Chapman and Lindzen 1970).

Diurnal variations over the tropical oceans are strongly apparent in heavy rainfall and deep convective cloudiness, with an early morning maximum in most regions (cf. Ruprecht and Gray 1976; Gray and Jacobson 1977). The mass circulations associated with the diurnally varying deep convective systems also exhibit day–night changes, with strongest ascent within the cloud cluster and descent in adjacent clear regions in the early morning (McBride and Gray 1980). Recently, the large-scale nature of the diurnal rainfall cycle over the tropical oceans has been revealed by satellites (cf. Hendon and Woodbury 1993; Janowiak et al. 1994). These studies show that the regions of time-mean deep convection (e.g., the intertropical and South Pacific convergence zones) exhibit the most pronounced diurnal variability.

Several complementary mechanisms have been proposed to explain the diurnal cycle in deep convective rainfall over the tropical oceans including day–night variations in tropospheric radiative cooling rates (Gray and Jacobsen 1977; Foltz and Gray 1979), cloud-radiation interactions (Randall et al. 1991; Xu and Randall 1995), and daytime heating of the sea surface (Hendon and Woodberry 1993; Chen and Houze 1997). However, the relative importance of these processes has not yet been resolved.

With the exception of the satellite-based estimates of rainfall, the large-scale spatial patterns of daily atmospheric circulation variations over the tropical oceans

* Current affiliation: National Center for Atmospheric Research, Boulder, Colorado.

[1] In this study, the term ''daily'' refers to all variations within a 24-h period, and the adjectives ''diurnal'' and ''semidiurnal'' refer to the first and second harmonics of the daily cycle, respectively.

Corresponding author address: Dr. Clara Deser, Climate and Global Dynamics Division, NCAR, P.O. Box 3000, Boulder, CO 80307-3000.
E-mail: cdeser@ucar.edu

are not known. An unprecedented observing network now exists for the documentation of daily variations of near-surface winds across the tropical Pacific: the Tropical Atmosphere–Ocean (TAO) moored buoy array. In this study, approximately 3 yr of hourly measurements from nearly 60 buoys between 165°E and 95°W are used to document the large-scale climatological daily variations in the low-level atmospheric circulation. We address the following issues. What are the spatial patterns of the climatological daily wind variations across the tropical Pacific? Are there associated large-scale daily changes in horizontal wind divergence? What is the magnitude and phase of the climatological daily wind and divergence variations? Are there seasonal and interannual modulations of the daily wind patterns? What are the relative contributions of the diurnal and semidiurnal harmonics to the mean daily wind cycles? A pilot study by Deser (1994) used a limited subset of the TAO data to examine similar issues in the eastern equatorial Pacific.

2. Data and methods

The TAO array was designed to monitor upper-ocean thermal conditions and surface atmospheric properties for improved prediction of the El Niño–Southern Oscillation cycle (Hayes et al. 1991; McPhaden 1993). Beginning with two buoys in late 1983, the array was fully implemented in December 1994 with 70 moorings distributed within 8° of the equator and spaced approximately every 15° of longitude across the Pacific basin (see McPhaden 1993). Winds are sampled at 2 Hz for 6 min every hour centered on the hour at ~3.8 m above the sea surface using cup-and-vane or propeller-and-vane assemblies [see McPhaden and Hayes (1990) and Hayes et al. (1991) for more details]. The expected instrumental errors are typically ~0.1 m s^{-1}, with maximum calibration residuals less than 0.2 m s^{-1} for any particular instrument, based on pre- and postdeployment calibration tests (McPhaden and Hayes 1990; Freitag et al. 1991). The hourly wind data are recorded on cassette tape or solid-state memory devices on board the buoys; the data archives are retrieved every 6 months to 1 yr and processed at the TAO project office at the Pacific Marine Environmental Laboratory in Seattle, Washington.

This study uses data from the period 1 January 1993–31 December 1996. The record lengths are highly variable from buoy to buoy, with frequent gaps within each record (Table 1). The average record length is 895 days (approximately 2.5 yr), with a maximum of 1335 days and a minimum of 412 days. Although it is desirable to use a common period of record for all the buoys, we felt it was more important to include as many sites as possible since our emphasis is upon the large-scale spatial patterns of daily variability. To minimize any potential aliasing of the seasonal cycle and interannual changes, the average daily march was computed for each

TABLE 1. Record length information for the TAO buoy wind data used in this study. For each buoy, the top entry lists the start and end dates (day/year), and the bottom entry lists the total number of days with data followed by the total number of days in the record (separated by a "/").

	165°E	180°	170°W	155°W	140°W	125°W	110°W	95°W
8°N	1/93–313/95	334/93–340/95	1/93–343/95	304/93–205/95	1/93–82/95	126/93–260/96	75/93–279/96	
	1038/1042	574/736	978/1072	466/631	707/811	1225/1229	961/1299	
5°N	1/93–194/96	88/93–15/96	1/93–206/96	1/93–183/95	290/93–243/96	59/93–40/96	73/93–280/96	267/94–267/96
	1282/1288	917/1022	1292/1300	907/912	926/1048	925/1076	885/1302	675/730
2°N	1/93–26/96	87/93–179/96	1/93–258/95	1/93–97/95	117/93–80/95	124/93–45/96	73/93–236/96	1/93–134/96
	790/1120	1083/1187	877/987	823/826	469/693	1013/1016	836/1258	412/1228
0°	1/93–104/94	86/93–336/95	1/93–209/96	1/93–360/95	1/93–252/95	1/93–174/96	129/93–222/95	1/93–293/96
	458/468	977/980	1289/1303	1081/1089	972/981	1259/1268	641/823	743/1387
2°S	1/93–191/96	85/93–180/96	1/93–346/95	307/93–219/96	1/93–251/95	1/93–239/96	1/93–284/96	1/93–130/96
	1112/1285	1133/1190	604/1075	827/1007	902/980	1234/1333	1094/1378	1219/1224
5°S	110/94–122/95	84/93–125/95	1/93–212/96	1/93–88/96	1/93–249/96	1/93–74/95	1/93–208/96	114/94–291/96
	378/377	608/771	836/1306	1025/1182	1335/1343	624/803	810/1302	457/907
8°S	1/93–188/96	326/93–334/95	1/93–354/95	1/93–217/96	1/93–217/96	1/93–253/96	69/93–135/96	227/94–132/96
	1203/1282	737/738	807/1083	1306/1311	0/1311	875/1347	1121/1161	634/635

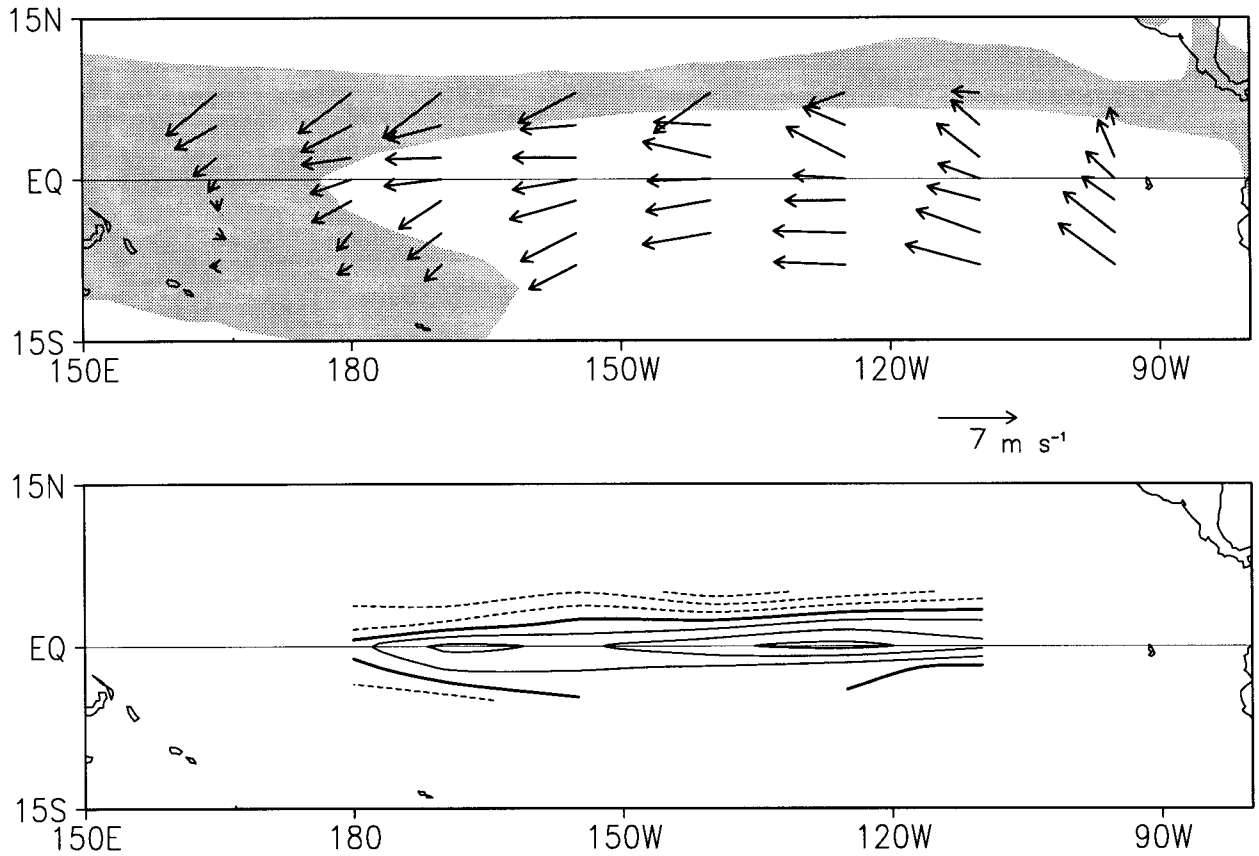

FIG. 1. (top) Mean near-surface wind vectors during 1993–96 from the TAO array superimposed upon the mean distribution of deep convection as inferred from OLR values less than 240 W m^{-2} (shading). The wind vector scale is indicated at the lower right (7 m s^{-1}). (bottom); divergence of the mean wind vectors above. Contour interval is 2×10^{-6} s^{-1}, with negative values dashed and the zero contour thickened.

2-month segment, from January–February 1993 to November–December 1996. Then, the mean daily marches from the three years were averaged for each bimonth. Finally, the resulting daily marches from the six ''long-term mean'' bimonths were averaged together to form the mean daily march during 1993–96.

3. Results

a. Mean daily march

Figure 1 shows the mean surface wind vectors during 1993–96 (top) and their divergence (bottom). Easterlies are present across the basin, with anticyclonic flow around the South Pacific subtropical high and northeast trade winds along 8°N. The low-level flow is strongly divergent along the equator (maximum values $\sim 6 \times 10^{-6}$ s^{-1}) and convergent north of $\sim$5°N [along the intertropical convergence zone (ITCZ)] and in the far southwestern Pacific (the South Pacific convergence zone; SPCZ). The locations of the wind convergence zones are qualitatively consistent with the mean distribution of deep convection as inferred from outgoing longwave radiation (OLR) values less than 240 W m^{-2} (Fig. 1, top).

The average daily march (in local time) of the zonal wind component at each buoy is shown in Fig. 2a. The mean standard error of an hourly wind average is 0.09 m s^{-1}. Semidiurnal fluctuations are evident at most locations, with peak-to-peak amplitudes of a few tenths of a m s^{-1}. The phase of the semidiurnal zonal wind variations is nearly uniform across the basin, with maxima around 0300–0400 and 1500–1600 local time (LT). Diurnal variations are evident at the three easternmost equatorial sites.

The average daily march of the meridional wind component (Fig. 2b) exhibits strong diurnal fluctuations with little semidiurnal variability. At many locations, the range of daily meridional wind variations exceeds 0.7 m s^{-1}, more than twice the daily range of the zonal wind variations. A general tendency for morning maxima north of the equator and evening maxima south of the equator can be noted. There does not appear to be any simple relationship between the phase of the diurnal cycle of the meridional wind and the direction of the mean meridional wind component. For example, along

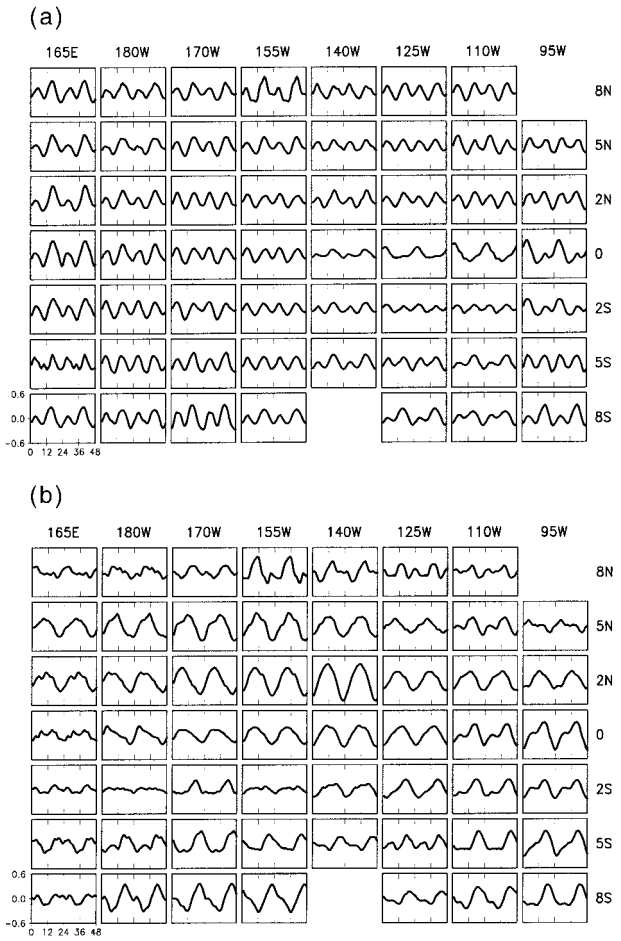

FIG. 2. (a) Average daily march of the zonal wind component during 1993–96 from the TAO array. All boxes are drawn to the same scale, with local time on the abscissa (0–48 h) and wind speed on the ordinate (-0.6 to 0.6 m s^{-1}), as shown in the lower-left box. The daily mean zonal winds have been removed from each site, and the hourly values smoothed with a three-point binomial filter. The 24-h period is repeated for clarity. Positive (negative) values indicate westerly (easterly) winds relative to the daily mean. (b) As in (a) but for the meridional wind component. Positive (negative) values indicate southerly (northerly) winds relative to the daily mean.

8°S, the maximum southerly winds occur near 1800 LT, although the mean meridional winds change from southerly in the east to northerly in the west (recall Fig. 1). A scatterplot of the phase of the diurnal cycle of meridional wind versus the mean meridional wind velocity (not shown) confirms the lack of a simple relationship: the linear correlation coefficient between these two quantities is not significantly different from zero.

b. Sample power spectra

Do the wind records exhibit distinct spectral peaks at the diurnal and/or semidiurnal frequencies, or are the daily fluctuations part of a continuum of high-frequency variability? We selected two buoys with long continous records to illustrate the nature of the wind power spectra and cross spectra. Figure 3a shows the power spectrum for the meridional wind component at 2°N, 125°W (top) and 8°S, 110°W (middle), and the squared coherence between them (bottom). Only submonthly timescales are shown. Analogous results for the zonal wind component are shown in Fig. 3b. The spectra are based on 1016 days of data (4 May 1993–13 February 1996), with five 2-day periods of missing data filled by linear interpolation.

The meridional wind spectra (Fig. 3a) exhibit significant peaks at the diurnal and synoptic (4–5 day) frequencies. However, the squared coherence is significant only at the diurnal frequency. The synoptic peak may be associated with mixed Rossby–gravity waves, a ubiquitous feature of the near-equatorial meridional wind field (Liebmann and Hendon 1990).

The zonal wind spectra (Fig. 3b) exhibit a general enhancement of power at timescales longer than about a week. A modest spectral peak is present at the semidiurnal frequency (and at the diurnal frequency at 8°S, 110°W). The squared coherence between the two zonal wind records is significant at the 99% level at the semidiurnal frequency and periods longer than about one week.

Power spectra for numerous other buoy wind records (not shown) confirm that significant diurnal and/or semidiurnal spectral peaks are present when the amplitude of the mean daily cycle (see Fig. 2) exceeds the mean standard error (approximately 0.1 m s^{-1}).

c. Harmonic analysis

The wind records shown in Figs. 2a and 2b were decomposed into diurnal and semidiurnal harmonics according to

$$X_k(t) = A_k \cos(\pi k/12t) + B_k \sin(\pi k/12t),$$

where X is the deviation of the zonal or meridional wind component from the daily mean, the index $k = 1$ ($k = 2$) refers to the diurnal (semidiurnal) harmonic, and t is time in hours. Here A_k and B_k were determined by the method of least squares (cf. Draper and Smith 1966).

The amplitudes and phases of the diurnal and semidiurnal wind harmonics at each buoy are listed in Table 2. Figure 4a (b) shows the amplitude and phase of the diurnal (semidiurnal) harmonic of the zonal wind component in vectorial format. The length of the arrow denotes the amplitude of the harmonic and the direction indicates the phase of the westerly wind maximum in local time. An arrow pointing due west indicates a local noon westerly maximum, with time increasing in the counterclockwise direction. Note that for the semidiurnal harmonic, an arrow oriented in the east–west direction indicates zonal wind maxima at midnight and noon local time.

The diurnal harmonic of the zonal wind component (Fig. 4, top) is generally weaker than the semidiurnal harmonic except at the three easternmost equatorial sites

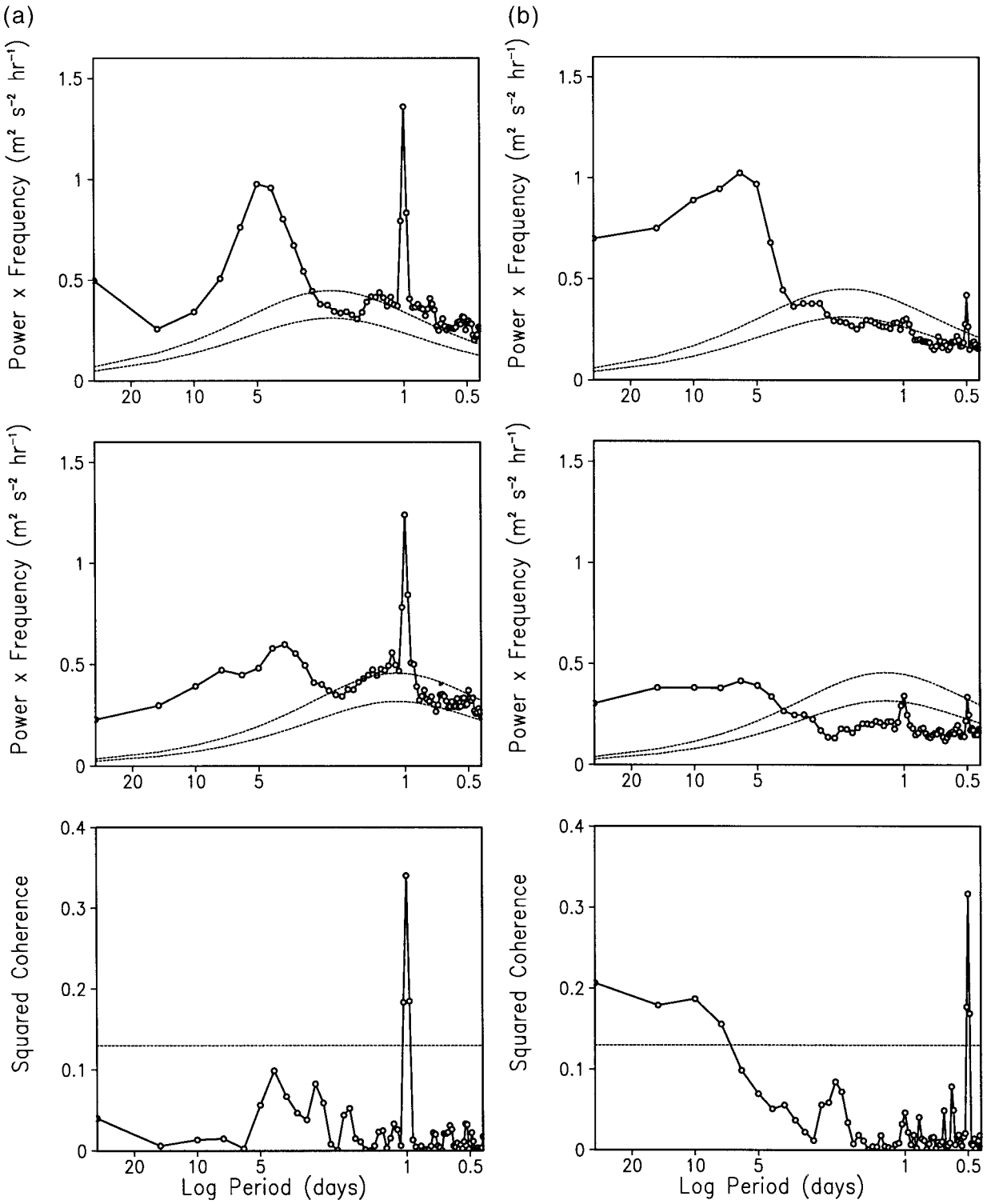

FIG. 3. (a) Power spectrum for the meridional wind component at 2°N, 125°W (top) and 8°S, 110°W (middle) based on 1016 days. The spectra are shown in variance conserving form: power spectral density multiplied by frequency along the ordinate, and log (period) in days along the abscissa. Only periods less than 1 month are shown. The thin dashed lines represent the spectra for the appropriate red noise background continuum and its 99% a priori confidence limit. The bottom panel shows the squared coherence between the two wind records. The thin dashed line is the 99% a priori significance level. (b) As in (a) but for the zonal wind component.

(see also Table 2), and shows no coherent spatial pattern. The average amplitude of the diurnal harmonic is 0.08 m s^{-1} compared to 0.15 m s^{-1} for the semidiurnal harmonic. The semidiurnal (diurnal) harmonic accounts for 68% (25%) of the total variance of the long-term daily march of the zonal wind component over the basin.

The semidiurnal harmonic of the zonal wind component is remarkably uniform in both phase and amplitude across the basin (Fig. 4, bottom; Table 2). The average phase (time of maximum westerly wind) ± one standard deviation is 0310 and 1510 LT ± 30 min, and the average amplitude is 0.15 m s^{-1} ± 0.04 m s^{-1}. The amplitude is somewhat larger in the west (0.18 m s^{-1} for 160°E–170°W) than in the east (0.12 m s^{-1} for 140°–110°W).

Figure 5 shows the results of harmonic analysis for the meridional wind component. An arrow pointing due west indicates a southerly wind maximum at local noon, with time increasing in the counterclockwise direction. The dominance of the diurnal harmonic over the semidiurnal harmonic is readily apparent, consistent with Fig. 2. The average amplitude of the diurnal (semidiurnal) harmonic is 0.19 m s^{-1} ± 0.09 m s^{-1} (0.07 m s^{-1} ± 0.03 m s^{-1}). The diurnal (semidiurnal) harmonic accounts for 82% (12%) of the total variance of the long-term daily march of the meridional wind component over the basin.

The diurnal meridional wind harmonic displays a distinctive spatial pattern, which in broadest terms may be described as a morning (0600–0900 LT) southerly wind maximum north of the equator, and an early evening (1800–2000 LT) southerly wind maximum south of the equator. Some differences may be noted between the western and eastern halves of the domain, particularly in the equatorial zone where the phase transition occurs. West of ~150°W, the diurnal cycle is weak along the latitude of the phase transition (2°S); east of ~150°W, the diurnal cycle is large in the equatorial zone, and characterized by a southerly wind maxima near local noon, making the phase transition more gradual than in the western Pacific.

The semidiurnal harmonic of the meridional wind component (Fig. 5b) exhibits a general pattern of cross-equatorial asymmetry (as evidenced by the horizontal bars north of the equator and vertical bars south of the equator), as well as a quadrature relationship to the zonal wind semidiurnal cycle (Fig. 4b). As discussed below, these phase relationships are consistent with the notion that the semidiurnal meridional winds result from the action of the Coriolis force.

The large-scale spatial patterns of the diurnal and semidiurnal wind harmonics are similar for the two solsticial seasons (not shown) and closely resemble those for the annual mean shown above.

The mean daily march of *wind speed* (not shown) is nearly identical to that of the zonal wind component, despite the generally lower amplitude of the mean daily cycle of the zonal versus meridional winds. The similarity of the mean daily marches of wind speed and zonal wind is due to the fact that the contributions of the zonal and meridional wind daily cycles to the wind speed daily cycle are weighted by their daily mean magnitudes (as can be shown formally with a Taylor series expansion), with the mean zonal winds being generally stronger than the mean meridional winds.

d. The semidiurnal wind cycle

It is well known that sea level pressure in the Tropics undergoes a strong semidiurnal variation, with amplitude ~1 mb and maximima ~0945 and 2145 LT (cf. Haurwitz and Cowley 1973; Hamilton 1980). This semidiurnal pressure cycle can be explained on the basis of atmospheric tidal theory (Chapman and Lindzen 1970). Briefly, atmospheric thermal tides are caused by heating due to the absorption of solar radiation by ozone in the stratosphere and to a lesser extent by water vapor and clouds in the troposphere. The ozone and water vapor heating excites vertically propagating modes that carry the signal from the stratosphere and upper troposphere to the ground. The surface tidal pressure signal is predominantly semidiurnal because 80% of the diurnal driving goes into modes whose energy is trapped near the level of forcing (Lindzen 1967).

Haurwitz and Cowley (1973) document the geographical pattern and seasonal variation of the semidiurnal pressure wave based on station data (note that a handful of island stations form the basis for their description over the tropical oceans). They show that the phase and amplitude of the semidiurnal pressure wave are approximately uniform within 20° of the equator, with slightly larger amplitude over the continents relative to the oceans. [The slight reduction in amplitude of the observed semidiurnal zonal wind fluctuations between 140°W and 110°W (recall Fig. 4b) is qualitatively consistent with the semidiurnal pressure field shown in Haurwitz and Cowley (1973), and may be related to the remoteness of this region from continental influences.]

The annual mean semidiurnal surface pressure cycle may be expressed as (Haurwitz and Cowley 1973)

$$P = 1.05 \cdot \cos^3(\theta) \cdot \sin(2t + 159°), \qquad (1)$$

where θ is latitude, t is local time in degrees, and the amplitude (1.05 mb) is characteristic of that over the tropical Pacific Ocean (see Haurwitz 1956). The 159° phase lag corresponds to pressure maxima at 0942 and 2142 LT. The pressure wave, shown graphically in Fig. 6, migrates westward with the sun, giving rise to zonal pressure gradients. The zonal wind (u) acceleration due to the semidiurnal pressure wave near the equator may be determined using a linear inviscid balance:

$$\delta u/\delta t = -1/\rho(\delta P/\delta x), \qquad (2)$$

where the symbols have their conventional meanings. Note that the zonal wind is out of phase with the pressure field and in quadrature with the pressure gradient field.

TABLE 2a. Amplitude, phase, and percent variance explained by the diurnal and semidiurnal harmonics of the mean daily march of the zonal wind component. For each buoy, the top entry lists the amplitude (m s^{-1}) and phase (hour and tenths in LT; separated by a "/") of the diurnal harmonic, the middle entry the amplitude (m s^{-1}) and phase (hour in LT; separated by a "/") of the semidiurnal harmonic, and the bottom entry the percent of the total mean daily variance explained (%) by the diurnal and semidiurnal harmonics (separated by a "/"). For example, at 8°N, 165°E, the amplitude and phase of the diurnal (semidiurnal) harmonic are 0.11 m s^{-1} (0.20 m s^{-1}) and 1218 LT (1506 LT), respectively; and the variance explained by the first (second) harmonic is 21% (74%).

	165°E	180°	170°W	155°W	140°W	125°W	110°W	95°W
8°N	0.11/12.3	0.09/14.7	0.08/18.5	0.17/17.2	0.05/21.5	0.07/19.0	0.07/20.6	
	0.20/15.1	0.14/15.5	0.16/15.2	0.19/14.8	0.14/15.5	0.17/15.4	0.17/15.4	
	21/74	25/64	18/75	39/51	11/77	13/85	13/84	
5°N	0.12/16.8	0.12/16.4	0.10/18.0	0.08/18.5	0.03/17.9	0.02/12.2	0.09/25.1	0.05/9.0
	0.17/15.2	0.11/14.9	0.18/15.3	0.15/15.4	0.12/15.4	0.13/14.8	0.18/15.5	0.15/16.4
	33/65	48/42	22/75	23/73	7/83	1/92	18/76	8/84
2°N	0.18/16.6	0.10/16.9	0.03/20.4	0.05/21.8	0.09/16.9	0.07/18.0	0.06/18.7	0.07/10.6
	0.19/15.3	0.16/15.1	0.19/15.5	0.14/15.5	0.14/15.2	0.12/15.0	0.16/15.5	0.18/15.5
	45/51	29/69	3/93	11/84	27/63	22/75	11/84	14/81
0°	0.16/16.0	0.08/16.8	0.07/20.7	0.06/21.5	0.06/14.3	0.11/24.6	0.19/24.2	0.20/25.2
	0.22/15.3	0.19/15.4	0.17/15.2	0.15/15.5	0.06/15.0	0.06/13.4	0.04/13.1	0.15/14.8
	32/60	15/79	12/85	13/81	49/41	79/19	89/5	62/36
2°S	0.11/17.2	0.05/21.7	0.09/21.8	0.04/19.3	0.06/15.2	0.03/23.8	0.03/19.9	0.12/25.1
	0.19/15.8	0.19/15.1	0.16/15.1	0.13/15.0	0.10/15.1	0.08/14.6	0.08/14.9	0.13/15.4
	24/69	6/92	22/74	8/88	23/71	16/77	9/78	44/53
5°S	0.01/18.5	0.03/19.2	0.08/13.5	0.03/15.5	0.10/14.7	0.05/10.8	0.10/13.9	0.03/10.3
	0.14/15.2	0.21/14.6	0.20/15.2	0.16/15.3	0.12/15.4	0.13/15.2	0.10/15.6	0.19/15.3
	0/54	1/92	12/83	2/93	39/57	13/79	46/49	2/89
8°S	0.13/13.0	0.07/12.8	0.13/12.1	0.09/16.1		0.14/13.3	0.11/11.4	0.13/14.8
	0.17/14.3	0.18/15.1	0.25/15.1	0.14/15.6		0.11/14.8	0.10/15.3	0.18/15.4
	35/62	11/80	20/73	31/66		58/40	51/47	35/62

The zonal wind computed from (1) and (2) is compared to the observed semidiurnal zonal wind in Fig. 7. (The amplitude and phase of the observed semidiurnal zonal wind was obtained by averaging the semidiurnal harmonics at all the buoys excluding the three equatorial sites between 140°W and 110°W.) There is good agreement between the observed and modeled semidiurnal zonal wind variations both in amplitude and phase. The observed winds are slightly weaker (0.16 m s^{-1} vs 0.18 m s^{-1}) and earlier (1520 LT vs 1540 LT) compared to the model winds. It remains to be seen whether surface frictional effects (not included in the simple model) can account for these small differences.

The three equatorial buoys between 140°W and 110°W exhibit highly suppressed semidiurnal fluctuations (Figs. 2a and 4b). We speculate that the stable thermodynamic conditions in the planetary boundary layer in this region (cf., Wallace et al. 1989; Deser and Wallace 1990; Bond 1992) may inhibit the propagation of the semidiurnal tidal signal down to the sea surface.

Are the meridional wind semidiurnal variations consistent with the semidiurnal pressure field? To first order, the inviscid meridional momentum balance is

$$\delta v/\delta t = -1/\rho(\delta P/\delta y) - fu, \qquad (3)$$

where f is the Coriolis parameter (note that the Coriolis term is of similar magnitude to the pressure gradient term in the meridional momentum balance). Since the meridional pressure gradient and Coriolis force are in phase with each other and in quadrature with the zonal pressure gradient term (recall Fig. 6), the meridional wind acceleration will be in quadrature with the zonal wind acceleration. Further, the semidiurnal meridional wind variations should be asymmetric about the equator, and identically zero at the equator. These characteristics are generally consistent with the observations shown in Fig. 5b.

Table 3 lists the amplitude and phase of the observed and modeled semidiurnal meridional wind perturbations at 8°N and 8°S. The observed winds are out of phase, as predicted from (3), with nearly identical magnitudes (0.065 m s^{-1}). Note that the phases (0520 and 1130 LT) are approximately 1 h earlier than those expected from a quadrature relationship with the zonal wind perturbation (Table 3). The modeled semidiurnal meridional wind variations are nearly identical to the observations in amplitude and show the expected phases (0645 LT and 1245 LT).

SEMIDIURNAL VARIATION OF SURFACE WIND DIVERGENCE

The semidiurnal cycle of surface wind divergence may be reconstructed from the semidiurnal harmonics of the zonal and meridional wind components. The resulting amplitude of the semidiurnal divergence averaged across the basin is 0.9×10^{-7} s^{-1}, with maximum convergence at 0620 and 1820 LT (not shown).

Several studies have reported a semidiurnal variation in rainfall over the tropical western Pacific using mea-

TABLE 2b. As in Table 2a but for the meridional wind component.

	165°E	180°	170°W	155°W	140°W	125°W	110°W	95°W
8°N	0.09/1.8 0.07/12.8 52/28	0.12/9.4 0.01/17.8 69/1	0.11/14.9 0.08/13.1 61/29	0.23/8.6 0.17/9.1 58/30	0.16/14.5 0.11/23.7 62/29	0.07/12.8 0.13/11.6 18/61	0.07/8.6 0.10/12.4 27/59	
5°N	0.20/7.8 0.04/12.6 92/4	0.27/8.3 0.02/22.8 93/0	0.29/9.1 0.08/13.7 89/8	0.31/9.6 0.04/14.1 92/2	0.25/9.7 0.04/13.4 95/2	0.15/7.3 0.01/21.3 88/0	0.14/11.2 0.12/13.5 53/41	0.09/29.0 0.07/13.2 49/29
2°N	0.20/8.7 0.06/13.7 82/9	0.23/6.7 0.06/14.1 91/6	0.31/6.2 0.05/15.5 96/2	0.33/8.8 0.05/15.8 96/2	0.44/9.5 0.06/15.0 98/2	0.23/9.8 0.02/16.1 98/0	0.23/10.0 0.05/14.4 93/5	0.21/11.4 0.01/22.9 93/0
0°	0.09/11.2 0.05/16.0 45/17	0.16/5.7 0.09/14.6 73/20	0.15/7.7 0.04/15.4 93/5	0.20/8.4 0.03/15.9 96/2	0.25/10.2 0.04/16.0 96/3	0.22/11.7 0.04/16.2 96/3	0.17/13.0 0.14/15.3 59/39	0.26/12.1 0.14/15.7 76/22
2°S	0.06/18.6 0.05/15.1 42/33	0.04/9.4 0.03/15.9 37/20	0.14/15.7 0.07/15.8 72/18	0.05/11.7 0.04/17.1 48/32	0.14/12.8 0.05/17.7 84/12	0.20/14.8 0.06/17.1 92/7	0.18/15.5 0.09/16.4 76/21	0.16/12.5 0.11/15.9 66/33
5°S	0.14/21.5 0.08/16.2 62/20	0.15/16.5 0.09/17.8 61/22	0.25/19.5 0.07/7.7 89/8	0.17/19.9 0.06/18.5 86/9	0.13/20.4 0.07/18.7 75/21	0.09/17.4 0.12/16.8 32/60	0.21/18.1 0.10/18.1 81/17	0.24/14.4 0.11/17.0 81/16
8°S	0.10/21.2 0.07/16.1 55/26	0.25/17.7 0.12/14.9 76/17	0.28/19.9 0.10/17.7 86/10	0.28/21.9 0.08/19.1 90/7		0.13/19.5 0.05/18.0 81/14	0.24/18.7 0.07/16.7 88/8	0.24/17.7 0.10/17.5 83/15

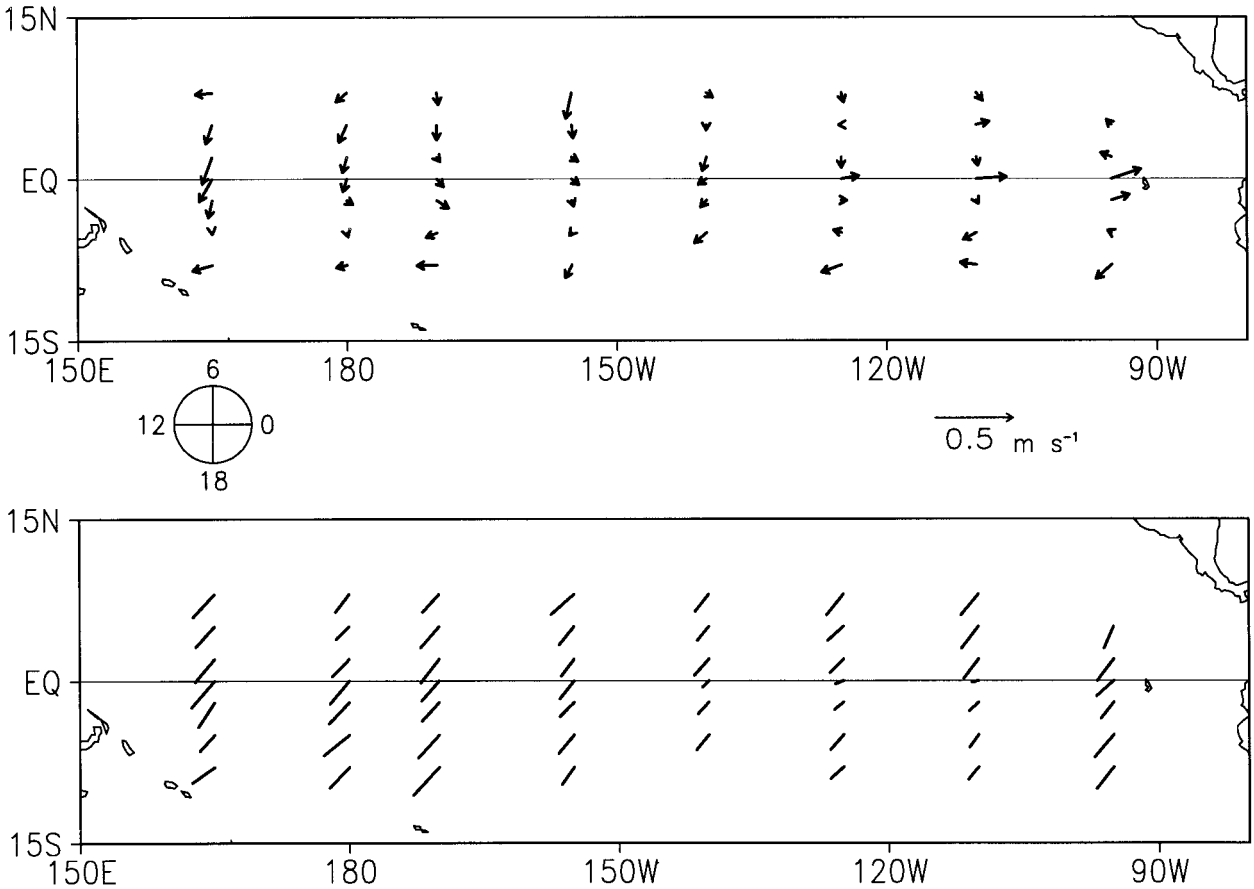

FIG. 4. (top) Vector representation of the amplitude and phase of the diurnal harmonic of the zonal wind component during 1993–96. The length of the arrow denotes the amplitude of the harmonic (m s^{-1}) and the direction indicates the phase in local time. An arrow pointing due west (south, east, north) indicates a westerly wind maximum at local noon (1800, 0000, 0600 LT). The wind vector scale is indicated at the lower right (0.5 m s^{-1}). (bottom) As in the top panel but for the semidiurnal harmonic of the zonal wind component. The wind vector scale is the same for both panels.

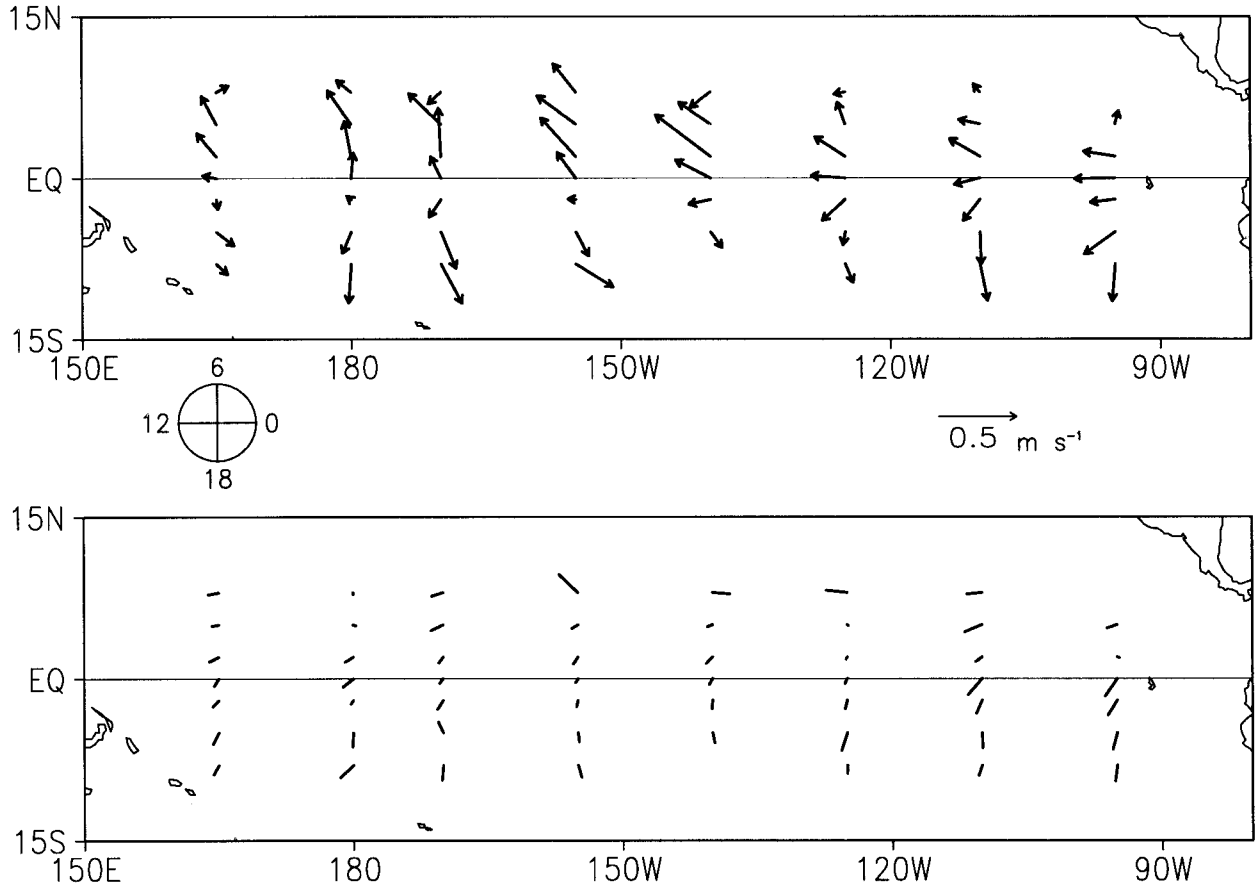

FIG. 5. (top) As in Fig. 4 but for the diurnal harmonic of the meridional wind component. An arrow pointing due west (south, east, north) indicates a southerly wind maximum at local noon (0600, 0000, 0600 LT). The wind vector scale is indicated at the lower right (0.5 m s^{-1}). (bottom) As in the top panel but for the semidiurnal harmonic of the meridional wind component. The wind vector scale is the same for both panels.

surements from small atolls (Hamilton 1981; Gray and Jacobson 1977) and aboard ships (RR97) where heat island effects are minimized. These studies indicate a semidiurnal rainfall rate amplitude of ~0.3–1 mm day^{-1} and a phase (time of maximum) near 0300–0400 LT and 1500–1600 LT.

The observed semidiurnal surface wind convergence maxima evidently *follow* the semidiurnal rainfall maxima in the tropical western Pacific by about 2 h. In addition, the nearly constant phase and amplitude of the semidiurnal zonal wind variations through the depth of the free troposphere (Williams et al. 1992) suggests that there is no appreciable vertical velocity associated with the semidiurnal pressure oscillation (only a change in net tropospheric mass locally; see also Lindzen 1967). Thus, it is difficult to implicate the semidiurnal thermal tide as the cause of the semidiurnal rainfall variation.

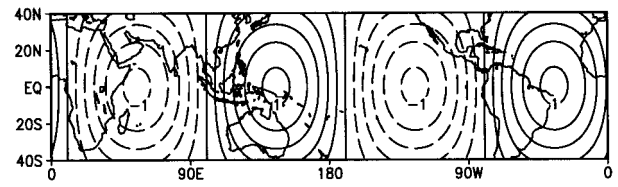

FIG. 6. The sun-synchronous semidiurnal cycle of sea level pressure (mb) at 0000 UTC according to Haurwitz and Cowley (1973). Positive (negative) pressure perturbations relative to the daily mean are shown as solid (dashed) contours. Contour interval is 0.2 mb.

e. The diurnal wind cycle

Figure 8 shows the mean diurnal wind vector deviations relative to the daily means at 0700, 1300, 1900, and 0100 LT. The wind vectors were reconstructed from the phase and amplitude of the diurnal harmonics of both wind components and smoothed in the zonal direction with a three-point binomial filter. The corresponding diurnal wind divergence fields are shown in Fig. 9. The divergences were computed from the reconstructed wind vectors in UTC, and then converted back to LT for display. At 0700 LT, the wind vectors show a general pattern of southerly flow relative to the daily mean at and north of the equator, and northerly flow relative to the daily mean south of 2°S. This pattern

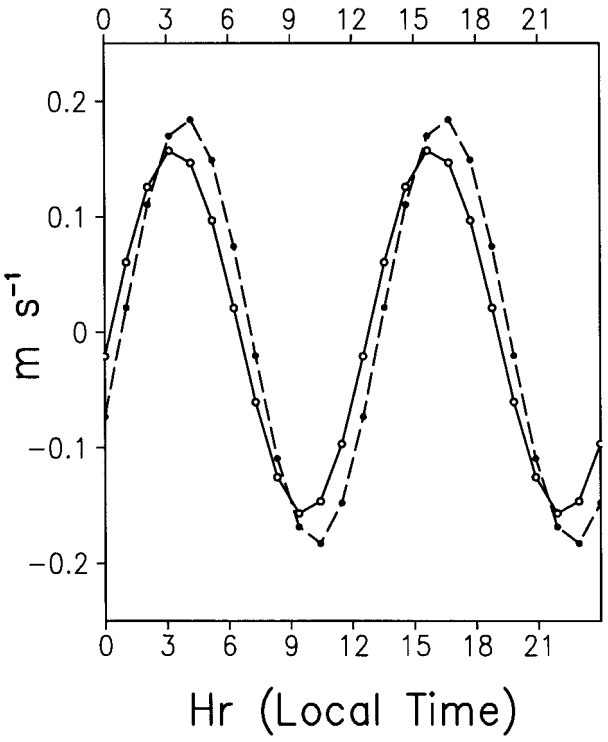

FIG. 7. Observed (solid curve) and modeled (dashed curve) semidiurnal variation of the zonal wind component (m s^{-1}) over the tropical Pacific in local time. The predicted wind is determined from the zonally averaged semidiurnal cycle of sea level pressure using a linear inviscid balance.

results in convergence north of ~3°N and divergence to the south relative to the daily mean (Fig. 9). Maximum divergence anomalies are 8×10^{-7} s^{-1} near 0°, 170°W. Six hours later (1300 LT), the meridional wind deviations have weakened substantially except over the eastern equatorial Pacific where strong southerly flow is evident. The wind pattern during this phase of the diurnal variation has little effect on divergence values in the western Pacific, while moderately enhancing the divergence (convergence) immediately to the south (north) of the equator in the eastern Pacific (Fig. 9). The wind patterns at 1900 and 0100 LT, shown for completeness, are reversed from those 12 h earlier.

1) ZONALLY SYMMETRIC COMPONENT

In view of the large zonally symmetric signal associated with the diurnal cycles of meridional wind and divergence, we show the mean diurnal cycle of the zonally averaged surface wind divergence across the Pacific as a function of latitude in Fig. 10. The diurnal cycle is approximately out of phase north and south of 3°N, with maximum convergence (divergence) at 5°N (0°–5°S) in the early morning (0600–0900 LT). The largest amplitude (6×10^{-7} s^{-1}) occurs at the equator. The diurnal cycle at 5°S is delayed relative to that at the equator by several hours, with maximum divergence occuring at 0900–1100 LT.

Figure 11 shows the latitudinal profiles of zonally averaged wind divergence near the times of maximum deviation from the daily mean (0800 and 2000 LT). Note that the long-term mean wind divergence is included in these profiles. The divergent area near the equator strengthens and expands southward in the early morning relative to the early evening. The total equatorial divergence, as estimated from the area under the positive portions of the two curves normalized by the (daily) mean latitudinal extent with actual divergence (6.1×10^5 m) decreases from 2.45×10^{-6} s^{-1} at 0800 LT to 1.55×10^{-6} s^{-1} at 2000 LT, a morning to evening ratio of 1.6 or a 45% percent change relative to the daily mean. Presumably, this extra mass divergence in the early morning is compensated by convergence to the north and south of the domain (there is a hint of the compensation at 5°N along the southern edge of the ITCZ; Fig. 11).

2) WEST VERSUS EAST PACIFIC

In addition to a zonally symmetric signal, the diurnal cycles of meridional wind and divergence exhibit east–west differences. In particular, the west Pacific (165°E–170°W) shows more asymmetry about the equator, while the east Pacific (140°–95°W) exhibits a distinctive diurnal cycle in the equatorial zone (recall Fig. 5a). These regions may also be distinguished on the basis of their climatological conditions, as illustrated by the wind divergence and OLR distributions in Fig. 1. The west Pacific is characterized by off-equatorial convergence and deep convection in both hemispheres, while the east Pacific has a single convergence zone north of the equator.

The latitudinal profiles of total wind divergence near the extremes of the diurnal cycle (0700 LT and 1900 LT) in the west Pacific are shown in Fig. 12a. Compared to the zonal averages (Fig. 11), the west Pacific exhibits more convergence north and south of the equator, and the equatorial divergence is more limited in strength and latitudinal extent. The total equatorial divergence

TABLE 3. Amplitude (m s^{-1}) and phase (hour in LT) of the observed and modeled semidiurnal zonal and meridional wind fluctuations at 8°N and 8°S.

	U (8°N and S avg)	**V** (8°N)	**V** (8°S)
Observed	0.16 m s^{-1}; 0320 LT	0.064 m s^{-1}; 0520 LT	0.067 m s^{-1}; 1130 LT
Modeled	0.18 m s^{-1}; 0340 LT	0.063 m s^{-1}; 0640 LT	0.063 m s^{-1}; 1240 LT

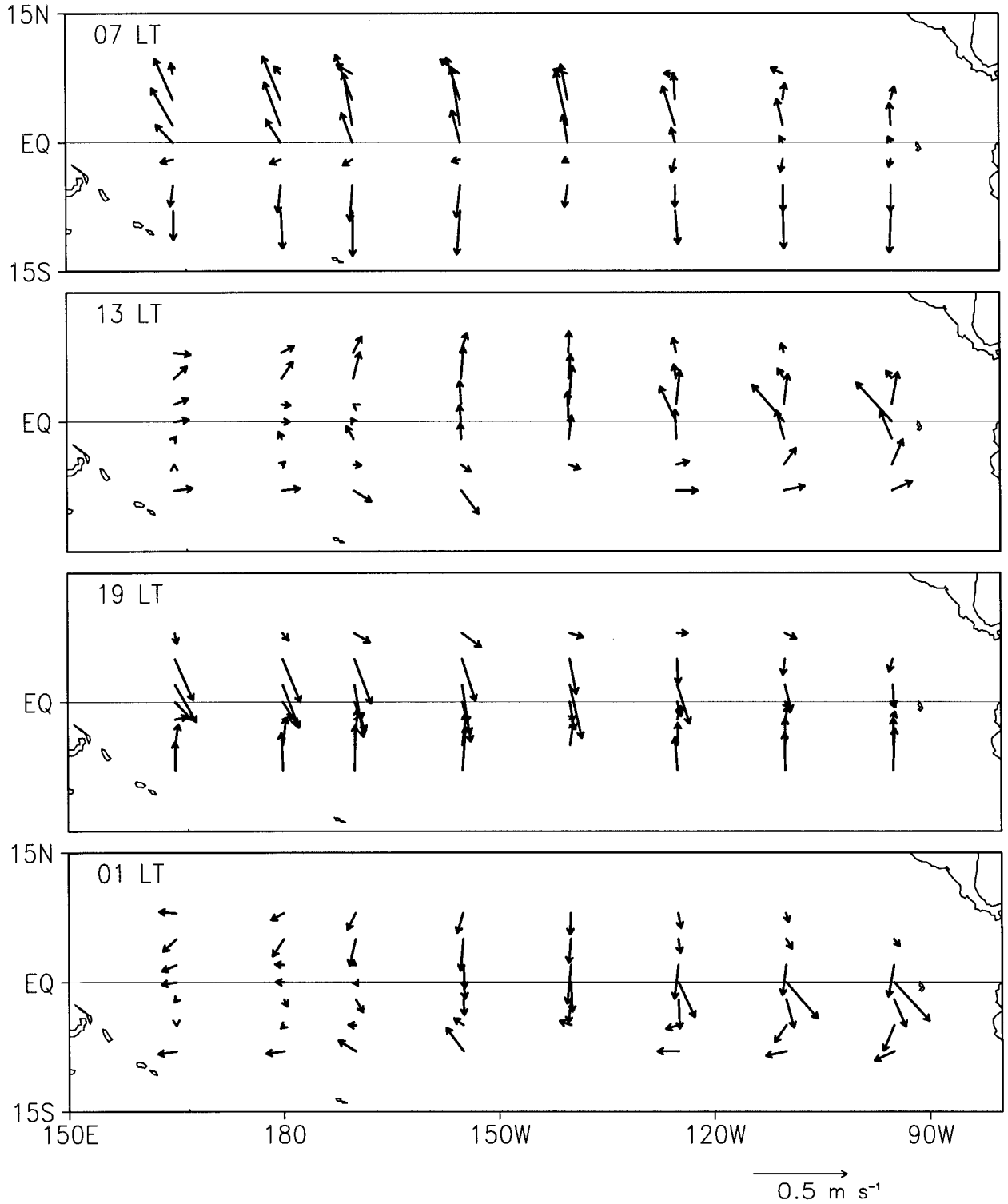

FIG. 8. Mean wind vector deviations from the daily means at 0700, 1300, 1900, and 0100 LT based on the period 1993–96. The wind vectors were smoothed in the zonal direction with a three-point binomial filter and represent 3-h averages centered on the times given above. The wind vector scale is shown at the lower right (0.5 m s^{-1}).

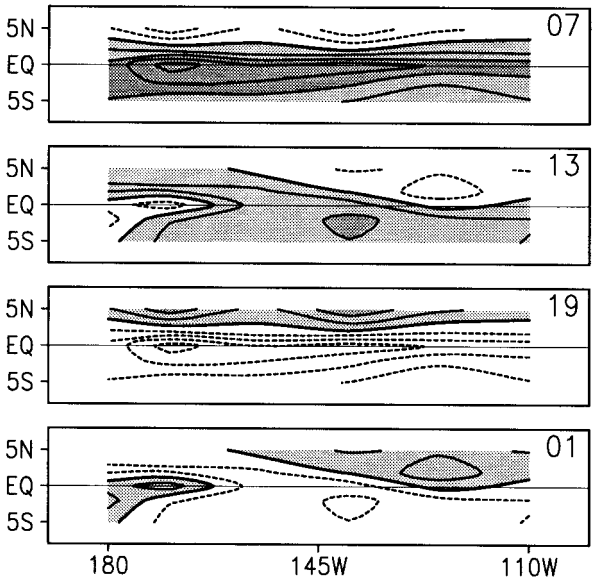

FIG. 9. As is Fig. 8 but for wind divergence. Contour interval is 2 $\times 10^{-7}$ s^{-1}, with negative values dashed and positive values shaded.

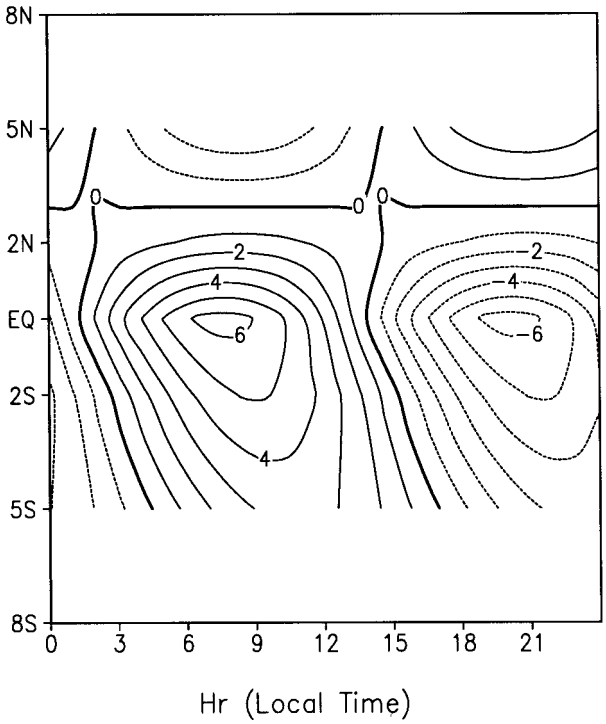

FIG. 10. Mean diurnal cycle (LT) of the zonally averaged surface wind divergence (10^{-7} s^{-1}) across the Pacific as a function of latitude based on the period 1993–96. The daily means at each latitude have been removed. Positive (negative) values indicate divergence (convergence) relative to the daily mean.

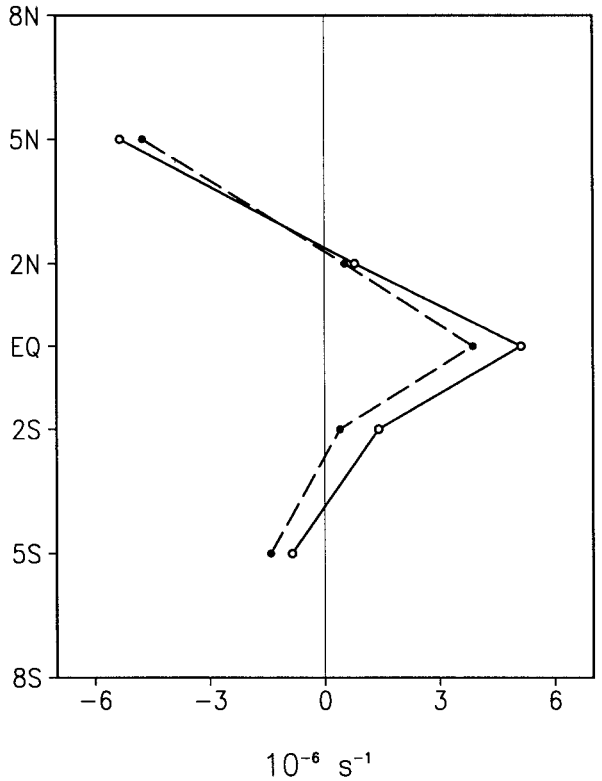

FIG. 11. The mean latitudinal profiles of zonally averaged surface wind divergence (10^{-6} s^{-1}) across the Pacific at the extremes of the diurnal cycle: 0800 LT (solid curve) and 2000 LT (dashed curve).

is 2.14 $\times 10^{-6}$ s^{-1} at 0600 LT and 0.93 $\times 10^{-6}$ s^{-1} at 1800 LT, a morning to evening ratio of 2.3 or a 78% percent change relative to the daily mean. The relative day–night differences are substantially larger than those for the zonal average, although the mean divergence is less.

Figure 12b shows analogous results for the east Pacific, where the morning and evening maxima occur near 0900 and 2100 LT, respectively, 2 h later than in the west Pacific. The equatorial divergence is stronger than in the west Pacific and zonal mean, and there is no convergence south of the equator. The total equatorial divergence is 2.74 $\times 10^{-6}$ s^{-1} at 0900 LT and 2.01 $\times 10^{-6}$ s^{-1} at 2100 LT, a morning to evening ratio of 1.4 or a 31% percent change relative to the daily mean. The relative day–night differences are smaller than those for the zonal average, although the mean divergence is greater.

3) SEASONAL AND INTERANNUAL VARIATIONS OF THE DIURNAL CYCLE OF EQUATORIAL WIND DIVERGENCE

Figure 13 shows the amplitude and phase of the diurnal harmonic of equatorial wind divergence in the western Pacific (165°E–170°W) at 2-month intervals computed from the difference between the meridional

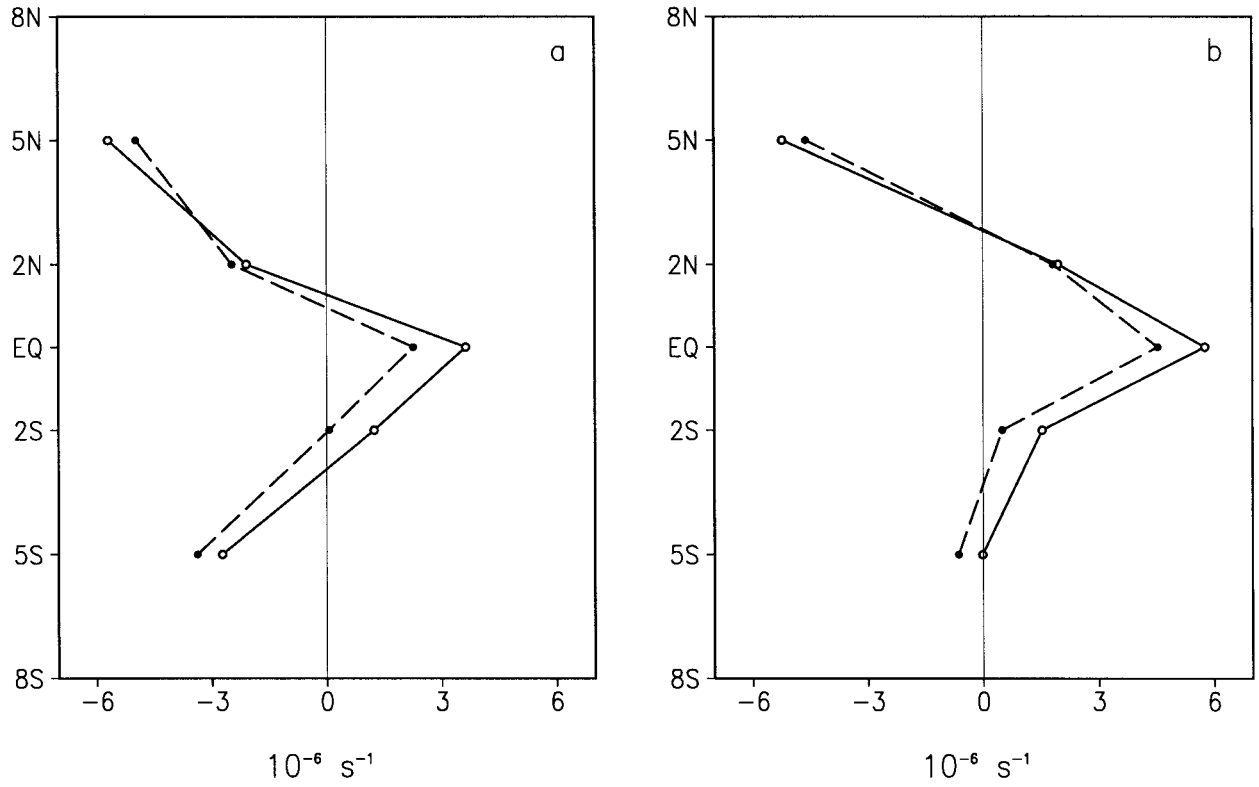

FIG. 12. The mean latitudinal profiles of surface wind divergence (10^{-6} s^{-1}) at the extremes of the diurnal cycle: (a) western Pacific at 0700 LT (solid curve) and 1900 LT (dashed curve) and (b) eastern Pacific at 0900 LT (solid curve) and 2100 LT (dashed curve).

winds at 2°–5°N and 5°–8°S. Note that it was not possible to reliably define the total wind divergence at each grid point for each 2-month segment due to large amounts of missing data. There is large secular variability in the diurnal amplitude of equatorial wind divergence in the western Pacific, with approximately twice as much diurnal variation during the last half of 1995 (8.1×10^{-7} s^{-1}) than during the previous year and a half (3.9×10^{-7} s^{-1}). The phase remains nearly constant during the entire period (0600–0800 LT).

Figure 14 shows the amplitude and phase of the diurnal cycle of equatorial wind divergence in the eastern Pacific (140°–95°W) at 2-month intervals, formed from the difference between the meridional winds at 0° and 8°S (there is little seasonal or interannual variation of the diurnal meridional winds north of the equator). A pronounced seasonal cycle is evident, with minimum diurnal amplitude ($2–3 \times 10^{-7}$ s^{-1}) in March–April and maximum ($\sim 6 \times 10^{-7}$ s^{-1}) in July–August. The phase of the diurnal cycle is fairly uniform throughout the year (0800–0100 LT).

The seasonal and interannual variations of the diurnal cycle of equatorial surface wind divergence are associated with changes in the mean divergence. In the western Pacific, there was enhanced equatorial wind divergence during the last half of 1995 compared to the previous 18 months (Fig. 15). The enhanced divergence was accompanied by increased OLR and reduced SST along the equator associated with the termination of warm episode conditions (not shown). In the eastern Pacific, the mean wind divergence between the equator and 8°S is considerably stronger in July–August than March–April as the South Pacific high strengthens and expands equatorward (Fig. 16). Thus, for both the interannual variations in the western Pacific and seasonal changes in the eastern Pacific, the diurnal amplitude of wind divergence varies in proportion to the strength of the mean divergence.

4. Discussion

a. Vertical and latitudinal extent of the diurnally varying circulation

We have shown that there is a strong diurnal variation in the low-level meridional wind field and associated equatorial mass divergence across the Pacific. Is there any evidence that the diurnal cycle in low-level equatorial divergence is linked to the day–night variation in heavy rainfall in the off-equatorial convergence zones? A simple moisture budget and preliminary analysis of the large-scale vertical motion field supports the notion of a diurnally varying deep tropospheric circulation that extends to at least 15° lat.

The extra low-level mass diverged from the equator in the early morning (see Figs. 8–11) is compensated

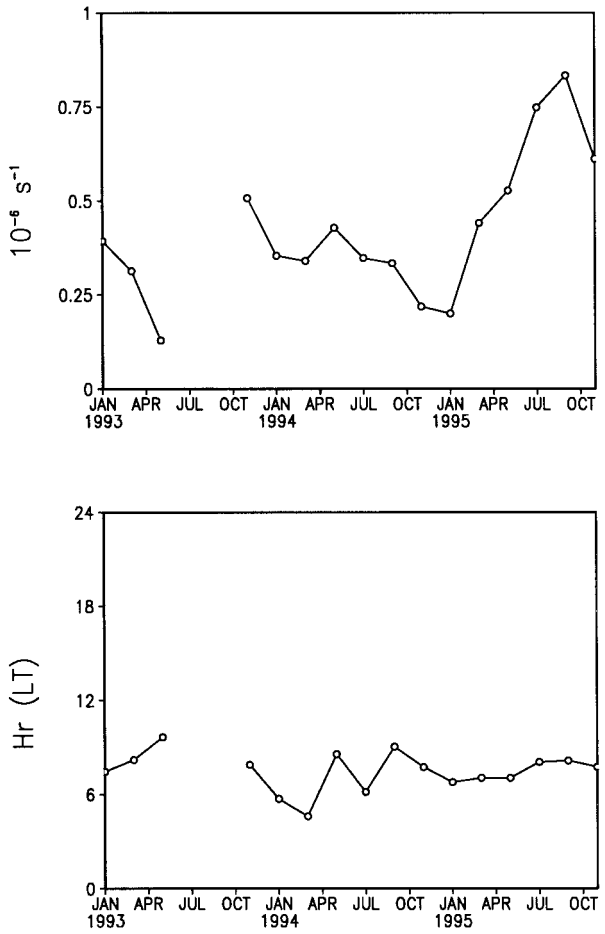

FIG. 13. Amplitude (top) and phase (bottom) of the diurnal harmonic of equatorial wind divergence in the western Pacific (165°E–170°W) at 2-month intervals computed from the difference between the meridional winds at 2°–5°N and 5°–8°S.

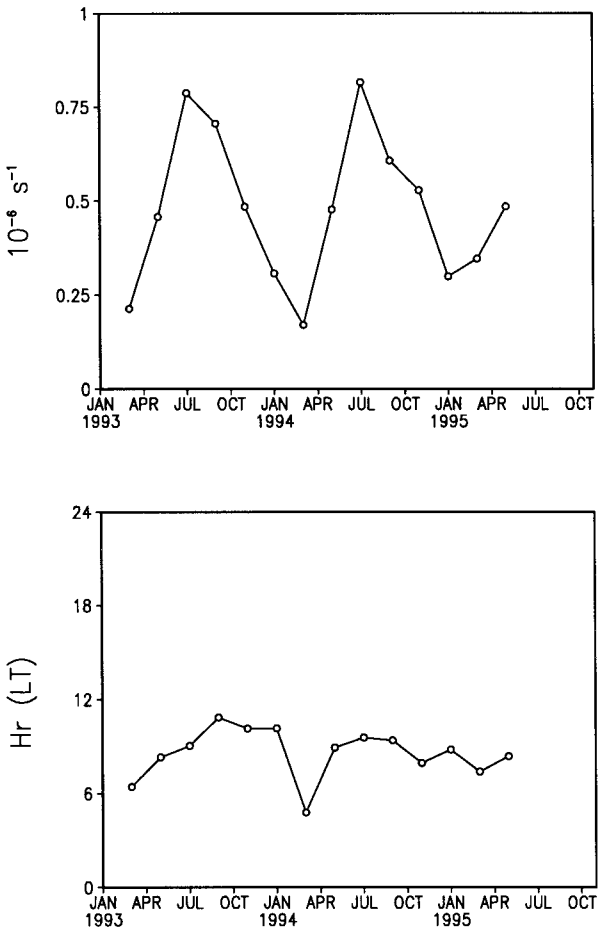

FIG. 14. As in Fig. 13 but for the eastern Pacific (140°–95°W), formed from the difference between the meridional winds at 0° and 8°S.

presumably by enhanced convergence to the north and south, although the buoy array does not extend far enough to verify this (there is a hint of the compensating mass convergence along 5°N at the southern edge of the ITCZ). Such a compensation would be consistent with the known early morning (0600–0900 LT) maximum in deep convection and heavy rainfall in the off-equatorial convergence zones (Hendon and Woodberry 1993; Gray and Jacobson 1977). One can make a simple estimate of the amplitude of the implied off-equatorial diurnal rainfall variation from the equatorial divergence diurnal amplitude (0.45×10^{-6} s^{-1}). Assuming that the divergence extends over a layer 200 mb deep, the average water vapor content of the converging air is 16 g kg^{-1}, and all of the converged moisture falls out as rain, the resulting diurnal rainfall amplitude is 1.4 mm day^{-1}, a value that compares favorably with direct estimates by Gray and Jacobson (1977) and others and indirect estimates by Hendon and Woodberry (1993) of 1–2 mm day^{-1}.

The above arguments rest on the assumption that the meridional overturning circulation in the tropical troposphere undergoes a diurnal modulation that links the low-level divergence along the equator with the precipitation maxima off the equator. To test this notion, a preliminary analysis of the diurnal cycle of large-scale vertical motion over the tropical Pacific was carried out using reanalysis data from the National Centers for Environmental Prediction (NCEP; Kalnay et al. 1996). The reanalyses are computed four times daily (at 0000, 0600, 1200, and 1800 UTC) on a 2.5° lat × 2.5° long grid. For the longitude band 180°–135°W in the central Pacific, the 0600 and 1800 UTC profiles correspond to 0600–0900 LT and 1800–2100 LT, respectively, near the extremes of the diurnal cycle of near-surface equatorial wind divergence.

Figure 17 shows the latitudinal profiles of morning and evening pressure vertical velocity (ω) averaged over the depth of the troposphere (925–200 mb) for 1995. Subsidence in the equatorial zone and rising motion in the SPCZ (7.5°–17.5°S) are more than twice as strong in the morning than in the evening. There is also enhanced morning subsidence in the northern subtropics.

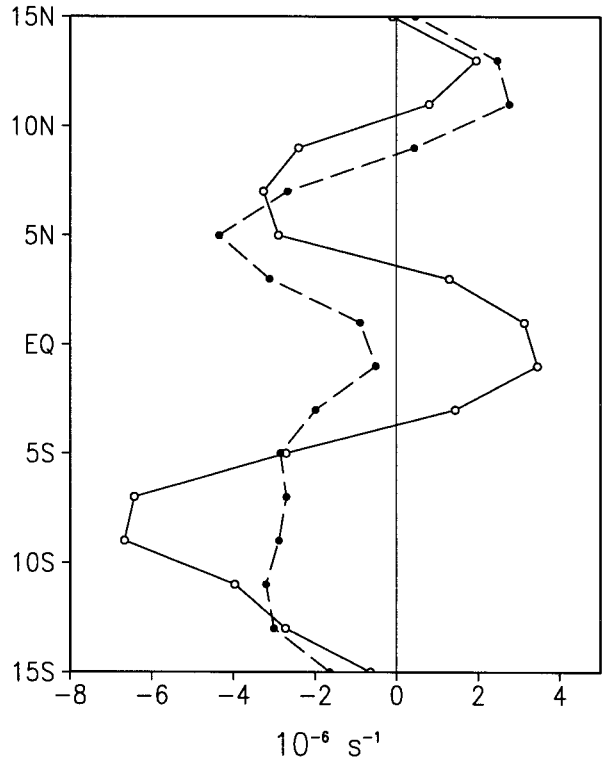

FIG. 15. Latitudinal profiles of mean surface wind divergence (10^{-6} s^{-1}) in the western Pacific (165°E–170°W) for July–December 1995 (solid curve) and January 1994–June 1995 (dashed curve) based on data from the Comprehensive Ocean–Atmosphere Data Set.

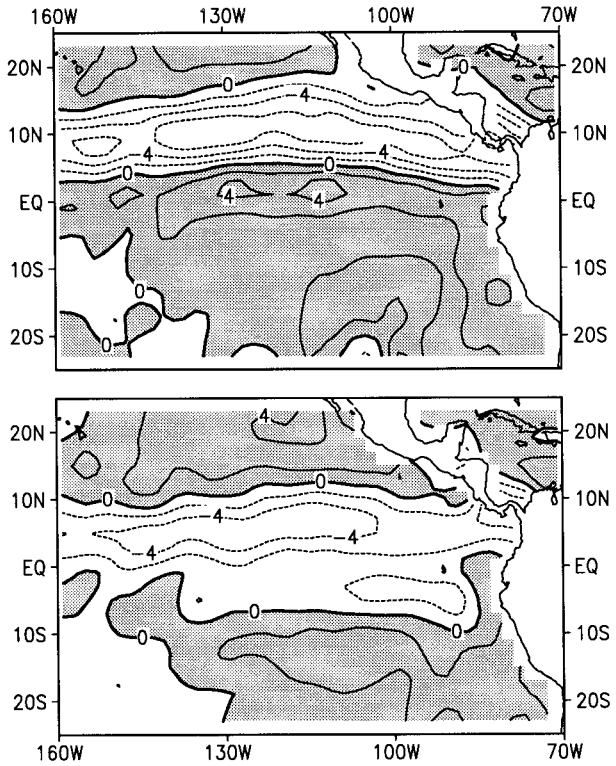

FIG. 16. Long-term mean surface wind divergence (10^{-6} s^{-1}) in the eastern Pacific for July–August (top) and March–April (bottom) based on data from the Comprehensive Ocean–Atmosphere Data Set. Contour interval is 2×10^{-6} s^{-1}.

The day–night changes in ω at the equator and SPCZ extend throughout the free troposphere (not shown). The magnitude of the morning-to-evening change in equatorial subsidence ($\omega \sim 0.02$ Pa s^{-1}) corresponds to a change in low-level divergence of $\sim 1 \times 10^{-6}$ s^{-1} for a boundary layer 200 mb deep: comparable to the buoy wind divergence estimate of 0.9×10^{-6} s^{-1}. Thus, the vertical motion field supports the notion that the diurnal cycle in near-surface wind divergence is linked to a deep meridional tropospheric circulation.

b. Comments on proposed radiative mechanisms for the diurnal cycle of deep convection

The role of radiative processes in driving day–night differences in oceanic deep convection has been emphasized by Gray and Jacobson (1977), McBride and Gray (1980), Foltz and Gray (1979), Randall et al. (1991), and Xu and Randall (1995). The work of Gray and colleagues emphasize the role of day–night variations in tropospheric longwave cooling in clear versus cloudy regions, while Randall and colleagues advocate the role of day–night variations in cloud-top shortwave absorption and longwave cooling.

Briefly, Gray and colleagues argue that day–night changes in net longwave cooling are largely compensated by subsidence warming. The radiatively driven day–night variation in subsidence rate will be larger for clear regions than cloudy areas since clouds reduce the net upward longwave flux. Horizontal contrasts in the radiatively driven subsidence rate will lead to a diurnal cycle in low-level mass divergence, with maximum convergence into the cloudy regions and divergence out of the clear regions toward dawn. While this mechanism depends only on the presence of adjacent cloud and cloud-free regions *in the mean,* Gray and colleagues note that the resulting diurnal cycle of convergence into the cloudy areas should result in increased deep convection and rainfall in the early morning.

In contrast, Randall and colleagues suggest that the clouds themselves force a diurnal cycle in rainfall by absorbing solar radiation during the day (thereby stabilizing lapse rates and inhibiting deep convection) and cooling by infrared emission during the night (thereby destabilizing lapse rates and promoting deep convection). It should be noted that this mechanism will also impact adjacent clear regions through conservation of mass.

Both radiative mechanisms should result in a diurnal circulation that is symmetric *with respect to the distribution of time-mean deep convection.* Figure 18 shows the mean buoy wind vector deviations from the daily means at 0700 and 1900 LT (taken from Fig. 8) super-

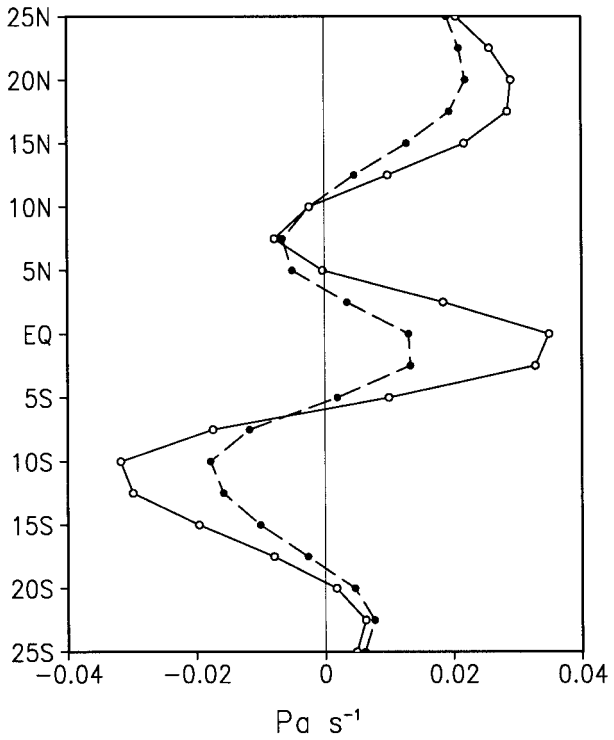

FIG. 17. Latitudinal profiles of pressure vertical velocity (ω; Pa s^{-1}) averaged over the depth of the troposphere (925–200 mb) at 0600–0900 LT (solid curve) and 1800–2100 LT (dashed curve) in the central Pacific (180°–135°W) based on the NCEP reanalyses for 1995. Positive values indicate downward motion.

imposed upon the time-mean distribution of deep convection (as given by OLR $<$ 240 W m^{-2}). Over the western tropical Pacific, the equatorial symmetry evident in the diurnal winds is also present in the mean rainfall pattern. That is, the flow of low-level air away from the clear equator into the regions of time-mean deep convection is strongest in the early morning: qualitatively consistent with both radiative mechanisms discussed above. However, in the eastern tropical Pacific, the equatorial symmetry in the winds is absent in the rainfall distribution. Hence, unless OLR is a poor indicator of deep clouds and high moisture contents in the eastern tropical South Pacific, it is difficult to see how the proposed radiative mechanisms can account for the equatorial symmetry in the diurnal wind cycles in the eastern tropical Pacific.

c. A possible role for SST in the diurnal cycle of low-level winds

The climatological distribution of sea surface temperature (SST) exhibits a narrow tongue of cold upwelled surface waters along the equator (Fig. 19, top). This ''equatorial cold tongue'' has a pronounced effect on the mean low-level atmospheric circulation, causing the winds to diverge above it (recall Fig. 1). [The cold waters induce lower temperatures in the atmospheric planetary boundary layer that are reflected hydrostatically as higher surface pressures (Lindzen and Nigam 1987).]

The mean diurnal amplitude of SST, constructed from the TAO buoys, exhibits a pronounced zonally symmetric component with maximum values along the equator (Fig. 19, bottom). The diurnal amplitude is two to three times stronger at the equator (0.16°C–0.27°C) than at 8°N or 8°S. The phase of the diurnal cycle is approximately uniform across the domain, with a mean of 1700 LT $\pm$ 10 min (not shown).

Driven by the diurnal cycle of incoming solar radiation, the diurnal variation of SST is also influenced by cloud amount and wind strength (Bond and McPhaden 1995; Webster et al. 1996). The reduction of the climatological mean cloudiness and wind speed along the equator is likely responsible for much of the spatial pattern of the SST diurnal amplitude shown in Fig. 19 (see Deser and Smith 1996).

The impact of the equatorial cold tongue on surface wind divergence *in the mean*, and the spatial pattern of the SST diurnal cycle, leads us to speculate that diurnal heating of the sea surface might contribute to reducing the zonally symmetric component of equatorial wind divergence during the day and enhancing it at night, as observed. Modeling experiments are needed to quantitatively test this hypothesis.

5. Conclusions

The climatological large-scale patterns of diurnal and semidiurnal near-surface wind fluctuations over the tropical Pacific have been documented using several years of hourly measurements from the TAO moored buoy array. The main results may be summarized as follows.

1) *Semidiurnal* variations account for 68% of the mean daily variance of the zonal wind component, while *diurnal* variations account for 82% of the mean daily variance of the meridional wind component.
2) The amplitude and phase of the semidiurnal zonal wind variations are nearly uniform across the basin, averaging 0.15 $\pm$ 0.04 m s^{-1} and 0310 $\pm$ 0030 LT, respectively.
3) The observed semidiurnal near-surface wind variations are dynamically consistent with the zonally averaged semidiurnal pressure field, which is forced by the atmospheric thermal tide in the stratosphere and upper troposphere.
4) The mean diurnal cycle of the meridional wind field exhibits a pronounced zonally symmetric component with opposite phase on either side of the equator. This pattern results in a diurnal variation of wind divergence in the equatorial zone with maximum divergence in the early morning (~0800 LT). The average amplitude of the diurnal cycle in zonal mean

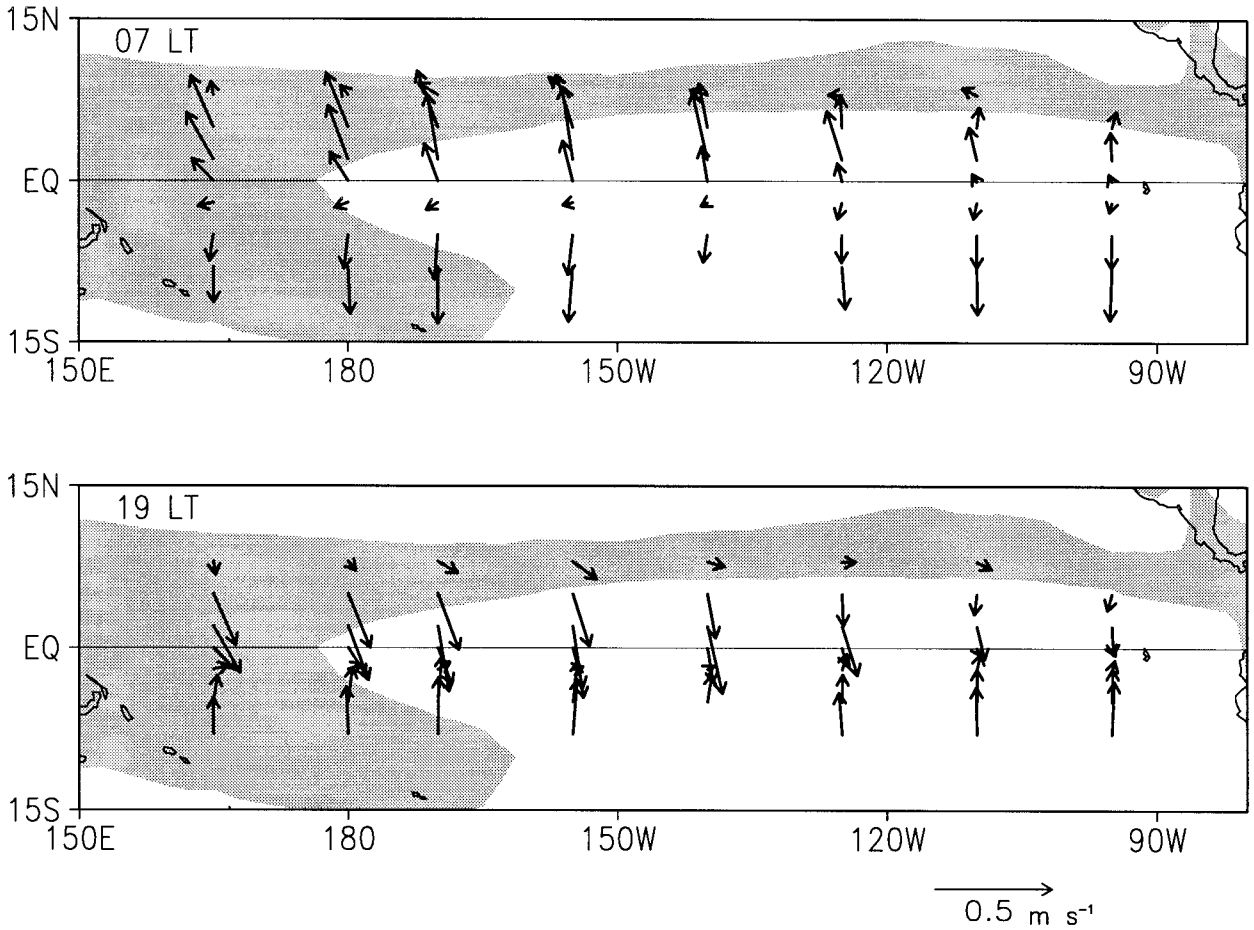

FIG. 18. Mean buoy wind vector deviations from the daily means at 0700 LT (top) and 1900 LT (bottom) superimposed upon the time-mean distribution of deep convection (as given by OLR < 240 W m^{-2}; shaded). The wind vector scale is shown at the lower right (0.5 m s^{-1}).

divergence is 0.45×10^{-6} s^{-1}, which corresponds to a day–night change of 45% relative to the daily mean. The relative day–night changes in near-surface wind divergence are larger in the west (78%) than in the east (31%), due mainly to differences in the daily mean divergence.

5) In addition to the zonally symmetric component, there are east–west differences in the structure of the diurnal meridional winds. In particular, the diurnal cycle at the equator is large in the eastern Pacific and negligible in the western Pacific. These differences may be related to the absence of a Southern Hemisphere convergence zone in the eastern tropical Pacific in the mean.
6) The diurnal cycle of equatorial wind divergence changes seasonally in the eastern Pacific and interannually in the western Pacific in proportion to the strength of the mean divergence.
7) We suggest that diurnal heating of the sea surface may play a role in forcing the zonally symmetric component of the diurnal cycle of equatorial wind divergence.

Future work

The wind data used in this study afford only a narrow equatorial view of the diurnal low-level circulation changes. A more complete description of the diurnal cycle throughout the global Tropics and subtropics is needed, including the vertical structure of the circulation changes. Wind profiles from the tropical island network of Doppler radars (Gage et al. 1991) may be particularily helpful in providing vertical structure information (see Gutzler and Hartten 1995; Williams and Avery 1996). Remotely sensed parameters such as tropospheric water vapor may provide insight into the large-scale nature of the diurnal circulation changes. In addition to observational studies, modeling work is needed to investigate the relative importance of radiative versus surface heating mechanisms in the diurnal cycle of the tropical maritime circulation.

As noted by Randall et al. (1991), the diurnal cycle may have implications for the time-mean surface energy budget and the partitioning of precipitation between land and sea. As such, the importance of the diurnal cycle

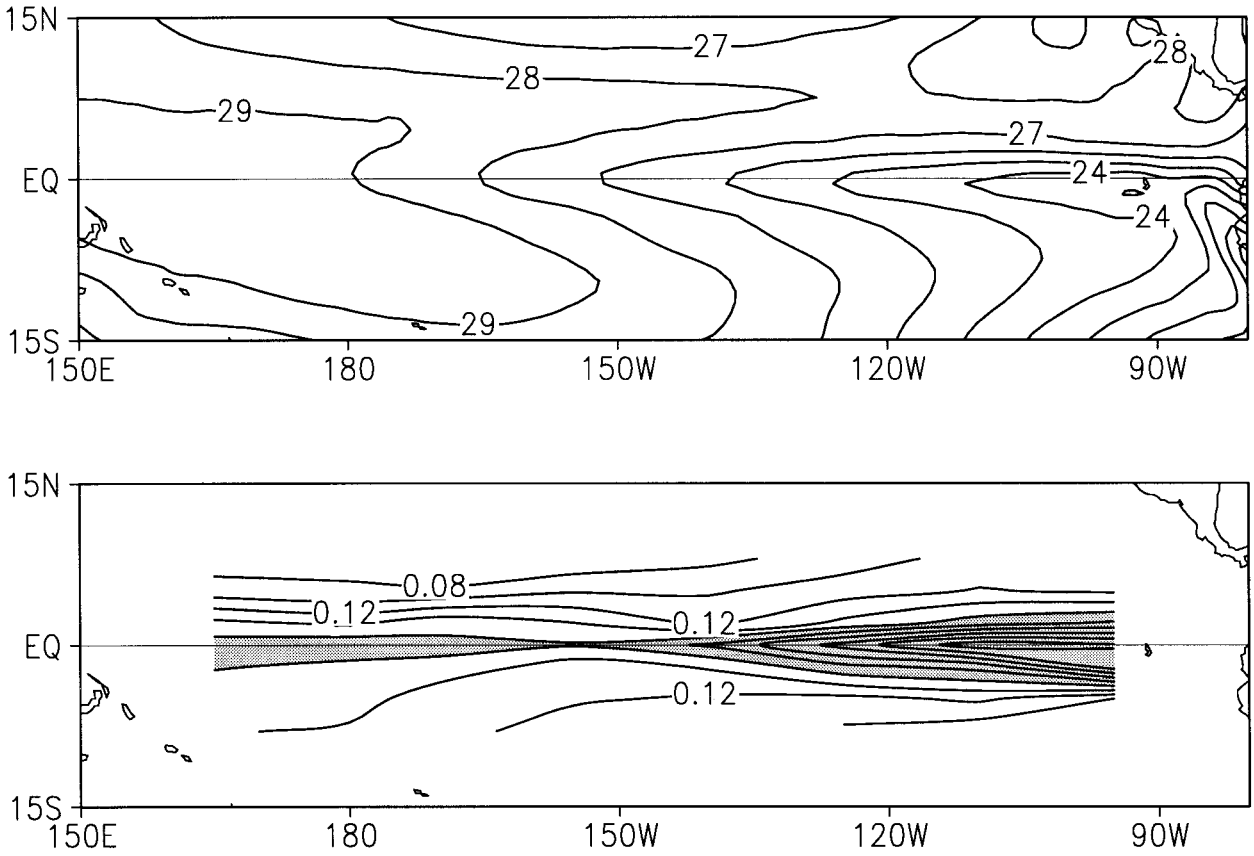

FIG. 19. (top) Mean SST distribution (°C) from Reynolds and Smith (1994). (bottom) Amplitude (°C) of the mean diurnal cycle of SST from the TAO buoys during 1993–96. Contour interval is 0.02°C, with values >0.16°C shaded. The buoys measure SST at a depth of 0.5 m.

may reach beyond the daily timescale to the mean state of the tropical atmosphere.

Acknowledgments. We wish to thank Mr. Michael S. Timlin for his invaluable assistance with the data processing and graphics. Discussions with Professor William Gray and Drs. John Knaff, John Scheaffer, and Jonathan Friedman are gratefully acknowledged. We are also indebted to Dr. Michael McPhaden and his staff at PMEL for providing the wind data used in this study. The graphics were produced with the GrADs package developed at the University of Maryland under the direction of Brian Doty. This study was supported by a grant from NOAA's Office of Global Programs. The comments of the anonymous reviewers helped us to improve the presentation of the results.

This paper is dedicated to the memory of Dr. Stanley P. Hayes, whose vision helped to establish the TAO array.

REFERENCES

Bond, N. A., 1992: Observations of planetary boundary layer structure in the eastern equatorial Pacific. *J. Climate*, **5,** 699–706.

——, and M. J. McPhaden, 1995: An indirect estimate of the diurnal cycle in upper ocean turbulent heat fluxes at the equator, 140°W. *J. Geophys. Res.*, **100,** 18 369–18 378.

Chapman, S., and R. S. Lindzen, 1970: *Atmospheric Tides.* D. Reidel, 200 pp.

Chen, S. S., and R. A. Houze, 1997: Diurnal variation and lifecycle of deep convective systems over the tropical Pacific warm pool. *Quart. J. Roy. Meteor. Soc.*, **123,** 357–388.

Deser, C., 1994: Daily surface wind variations over the equatorial Pacific Ocean. *J. Geophys. Res.*, **99,** 23 071–23 078.

——, and J. M. Wallace, 1990: Large-scale atmospheric circulation features of warm and cold episodes in the tropical Pacific. *J. Climate*, **3,** 1254–1281.

——, and C. A. Smith, 1996: Daily cycles of SSTs and surface winds over the tropical Pacific from the TAO moored buoy array. *Proc. 20th NOAA Climate Diagnostics Workshop*, Seattle, WA, NOAA, 256–259.

Draper, N. R., and H. Smith, 1966: *Applied Regression Analysis.* John Wiley and Sons, 407 pp.

Foltz, G. S., and W. M. Gray, 1979: Diurnal variation in the troposphere's energy balance. *J. Atmos. Sci.*, **36,** 1450–1466.

Freitag, H. P., M. J. McPhaden, C. H. Coho, and A. J. Shepherd, 1991: Equatorial wind, current and temperature data: 108°W to 140°W; April 1983 to October 1987. NOAA Data Rep. ERL PMEL-35, 116 pp.

Gage, K. S., G. G. Balsley, W. L. Ecklund, D. A. Carter, and J. R. McAfee, 1991: Wind profiler related research in the tropical Pacific. *J. Geophys. Res.*, **96,** 3209–3220.

Gray, W. M., and R. W. Jacobson Jr., 1977: Diurnal variation of deep cumulus convection. *Mon. Wea. Rev.*, **105,** 1171–1188.

Gutzler, D. S., and L. M. Hartten, 1995: Daily variability of lower

tropospheric winds over the tropical western Pacific. *J. Geophys. Res.*, **100,** 22 999–23 008.

Hamilton, K., 1980: The geographical distribution of the solar semidiurnal surface pressure oscillation. *J. Geophys. Res.*, **85,** 1945–1949.

——, 1981: Latent heat release as a possible forcing mechanism for atmospheric tides. *Mon. Wea. Rev.*, **109,** 3–17.

Haurwitz, B., 1956: The geographical distribution of the solar semidiurnal pressure oscillation. N.Y. University Meteor. Paper, 2(5), 36 pp.

——, and A. D. Cowley, 1973: The diurnal and semidiurnal barometric pressure oscillations: Global distribution and annual variation. *Pure Appl. Geophys.*, **102,** 193–222.

Hayes, S. P., L. J. Mangum, J. Picaut, A. Sumi, and K. Takeuchi, 1991: TOGA–TAO: A moored array for real-time measurements in the tropical Pacific Ocean. *Bull. Amer Meteor. Soc.*, **72,** 339–347.

Hendon, H. H., and K. Woodberry, 1993: The diurnal cycle of tropical convection. *J. Geophys. Res.*, **98,** 16 623–16 637.

Janowiak, J. E., P. A. Arkin, and M. Morrissey, 1994: An examination of the diurnal cycle in oceanic tropical rainfall using satellite and in situ data. *Mon. Wea. Rev.*, **122,** 2296–2311.

Kalnay, E., and Coauthors, 1996: The NCEP/NCAR 40-year reanalysis project. *Bull. Amer. Meteor. Soc.*, **77,** 437–471.

Liebmann, B., and H. H. Hendon, 1990: Synoptic-scale disturbances near the equator. *J. Atmos. Sci.*, **47,** 1463–1479.

Lindzen, R. S., 1967: Thermally driven diurnal tide in the atmosphere. *Quart. J. Roy. Meteor. Soc.*, **93,** 18–42.

——, 1968: The application of classical atmospheric tidal theory. *Proc. Roy. Soc. London*, **A303,** 299–316.

——, and S. Nigam, 1987: On the role of sea surface temperature gradients in forcing low-level winds and convergence in the Tropics. *J. Atmos. Sci.*, **44,** 2440–2458.

McBride, J. L., and W. M. Gray, 1980: Mass divergence in tropical weather systems. Paper I: Diurnal variation. *Quart. J. Roy. Meteor. Soc.*, **106,** 501–516.

McPhaden, M. J., 1993: TOGA–TAO and the 1991–93 El Niño–Southern Oscillation event. *Oceanography*, **6,** 36–44.

——, and S. P. Hayes, 1990: Variability in the eastern equatorial Pacific during 1986–88. *J. Geophys. Res.*, **95,** 13 195–13 208.

Morrissey, M. L., 1990: An evaluation of ship data in the equatorial western Pacific. *J. Climate*, **3,** 99–112.

Nitta, T., and S. Esbensen, 1974: Diurnal variations in the western Atlantic trades during BOMEX. *J. Meteor. Soc. Japan*, **52,** 254–257.

Pedder, M. A., 1978: Diurnal and semidiurnal variations in the A/B Scale-averaged wind fields during phase III of GATE. *Mon. Wea. Rev.*, **106,** 782–788.

Randall, D. A., Harshvardhan, and D. A. Dazlich, 1991: Diurnal variability of the hydrologic cycle in a general circulation model. *J. Atmos. Sci.*, **48,** 40–62.

Reynolds, R. W., and T. M. Smith, 1994: Improved global sea surface temperature analyses using optimum interpolation. *J. Climate*, **7,** 929–948.

Ruprecht, E., and W. M. Gray, 1976: Analysis of satellite-observed cloud clusters, Paper I and II. *Tellus*, **28,** 391–425.

Wallace, J. M., T. P. Mitchell, and C. Deser, 1989: The influence of sea surface temperature variability upon surface wind in the eastern equatorial Pacific: Seasonal and interannual variability. *J. Climate*, **2,** 1492–1499.

Webster, P. J., C. A. Clayson, and J. A. Curry, 1996: Clouds, radiation, and the diurnal cycle of sea surface temperature in the tropical western Pacific. *J. Climate*, **9,** 1712–1730.

Williams, C. R., and S. K. Avery, 1996: Diurnal winds observed in the tropical troposphere using 50 MHz wind profilers. *J. Geophys. Res.*, **101,** 15 051–15 060.

——, ——, J. R. McAfee, and K. S. Gage, 1992: Comparison of observed diurnal and semidiurnal tropospheric winds at Christmas Island with tidal theory. *Geophys. Res. Lett.*, **19,** 1471–1474.

Xu, K., and D. A. Randall, 1995: Impact of interactive radiative transfer on the macroscopic behavior of cumulus ensembles. Part II: Mechanisms for cloud-radiative interactions. *J. Atmos. Sci.*, **52,** 800–817.